Modeling and Simulation of an Unmanned Ground Vehicle Power System

John Broderick[a*], Jack Hartner[b], Dawn Tilbury[a], and Ella Atkins[a]

[a]The University of Michigan, Ann Arbor, MI, USA
[b]U.S. Army RDECOM-TARDEC, Warren, MI, USA

ABSTRACT

Long-duration missions challenge ground robot systems with respect to energy storage and efficient conversion to power on demand. Ground robot systems can contain multiple power sources such as fuel cell, battery and/or ultra capacitor. This paper presents a hybrid systems framework for collectively modeling the dynamics and switching between these different power components. The hybrid system allows modeling power source on/off switching and different regimes of operation, together with continuous parameters such as state of charge, temperature, and power output. We apply this modeling framework to a fuel cell/battery power system applicable to unmanned ground vehicles such as Packbot or TALON. A simulation comparison of different control strategies is presented. These strategies are compared based on maximizing energy efficiency and meeting thermal constraints.

Keywords: Unmanned Ground Vehicles, Power Systems, Hybrid Models

1. INTRODUCTION

Future robotic vehicles including both small unmanned ground vehicles (UGVs) and full-scale vehicles have multiple sources of power, including batteries, fuel cells, combustion engines, ultracapacitors, and solar cells, to allow for extended periods of operation. Fuel-based power sources have a higher specific energy than batteries, the reason most current automobiles are gasoline-powered. Batteries have many other advantages in terms of low noise profile, easy replacement, and direct energy conversion. Solar charging allows for harvesting of natural resources to increase total energy reserves. Mission duration may be maximized by using a combination of power systems. Long endurance is especially valuable for autonomous robots that can operate indefinitely without human contact.

To effectively integrate multiple power system components, we present a modeling framework that can be used to simulate and plan operation of UGV power systems. First, each component is individually modeled using either empirical or theoretical techniques. These models consider power component states, such as time of operation, state of charge, and temperature. For a given mission, the power demand is estimated and the power system models are combined to compute total energy use. As a part of the model, we also account for energy losses due to the operation of power system components. Losses include resistive heating in batteries and startup or shutdown power demands. In addition to full, nonlinear models for the UGV power system, we demonstrate a simplification process that can be used to reduce the models to linear dynamics. These simplified models can be used plan missions or roughly estimate power system operation for a desired mission.

In particular, we are motivated by a 200 W fuel cell manufactured by Ultra Electronics, Adaptive Materials, Inc. This particular fuel cell, as described in more detail in Section 3.1, can only be turned on or off, with no variation in the power produced when on, and requires several minutes and nontrivial power input to transition between on and off. These limitations on the fuel cell lead naturally to the proposed hybrid systems framework.

Using a model of this fuel cell connected to a battery, we simulate operation of the power system and evaluate different control strategies in terms of relative energy efficiency while maintaining constraints on other state variables. Section 4 considers different ways of operating the fuel cell based on the battery state of charge. The relative energy efficiency and thermal response of the battery are presented for each control strategy.

---

*corresponding author: `jabrod@umich.edu`

Report Documentation Page

1. REPORT DATE	2. REPORT TYPE	3. DATES COVERED
28 MAR 2014	**Journal Article**	**06-10-2013 to 11-02-2014**

4. TITLE AND SUBTITLE	5a. CONTRACT NUMBER
Modeling and Simulation of an Unmanned Ground Vehicle Power System	**W56HZV-04-2-001**
	5b. GRANT NUMBER
	5c. PROGRAM ELEMENT NUMBER

6. AUTHOR(S)	5d. PROJECT NUMBER
John Broderick; Jack Hartner; Dawn Tilbury; Ella Atkins	5e. TASK NUMBER
	5f. WORK UNIT NUMBER

7. PERFORMING ORGANIZATION NAME(S) AND ADDRESS(ES)	8. PERFORMING ORGANIZATION REPORT NUMBER
The University of Michigan,Fleming Administration Building,Ann Arbor,Mi,48109	**; #24584**

9. SPONSORING/MONITORING AGENCY NAME(S) AND ADDRESS(ES)	10. SPONSOR/MONITOR'S ACRONYM(S)
U.S. Army TARDEC, 6501 East Eleven Mile Rd, Warren, Mi, 48397-5000	**TARDEC**
	11. SPONSOR/MONITOR'S REPORT NUMBER(S)
	#24584

12. DISTRIBUTION/AVAILABILITY STATEMENT
Approved for public release; distribution unlimited

14. ABSTRACT
Long-duration missions challenge ground robot systems with respect to energy storage and e fficient conversion to power on demand. Ground robot systems can contain multiple power sources such as fuel cell, battery and/or ultra capacitor. This paper presents a hybrid systems framework for collectively modeling the dynamics and switching between these different power components. The hybrid system allows modeling power source on/or switching and different regimes of operation, together with continuous parameters such as state of charge, temperature, and power output. We apply this modeling framework to a fuel cell/battery power system applicable to unmanned ground vehicles such as Packbot or TALON. A simulation comparison of different control strategies is presented. These strategies are compared based on maximizing energy e ciency and meeting thermal constraints.

15. SUBJECT TERMS
Unmanned Ground Vehicles, Power Systems, Hybrid Models

16. SECURITY CLASSIFICATION OF:			17. LIMITATION OF ABSTRACT	18. NUMBER OF PAGES	19a. NAME OF RESPONSIBLE PERSON
a. REPORT **unclassified**	b. ABSTRACT **unclassified**	c. THIS PAGE **unclassified**	**Public Release**	**10**	

2. RELATED WORK

While current UGVs are almost universally battery powered, the UGV community has begun to investigate replacing or augmenting the battery with a fuel cell. Wilhelm et al. present a UGV powered exclusively by a fuel cell.[1] Their robot was quite small, using a 10 W fuel cell, and served as a proof of concept. Joh et al. present a humanoid robot powered by a fuel cell and a battery in parallel.[2] The authors demonstrate the use of their robot, including the use of the battery to supplement the fuel cell when the power demand exceeds the capacity of the fuel cell. However, the fuel cell is able to vary the power output to meet the demand and there is no discussion of charging the battery when power demands are low.

2.1 Hybrid Power Sources

Hybrid power sources are a major area of interest in the automotive industry.[3] Most existing systems are based on a combustion engine/battery hybrid. However, there are some initial investigations into a fuel cell/battery hybrid automobile.[4,5] Ceraolo et al. presents a general approach to hybrid power architectures for automobiles.[6] For cars, due to the fact that the engine produces mechanical power and the battery produces electrical power, one of the key design decisions is between a parallel, series, or more complex power connection.

The main objective of hybrid power controllers in the published literature is to increase fuel economy through limiting inefficiencies. For a series configuration, the generator can be run at any desired speed. Barsali et al. present one algorithm for this configuration.[7] If possible, they run the generator in an on-off mode of operation, with the generator operating at the most efficient point when on. They optimize the ratio of on-time to off-time and, based on a desired range of battery state of charge, the actual values of these times. In cases where the generator must be run constantly at a less efficient set point, the average battery level is held constant.

For parallel configurations, the speed of the engine cannot be chosen due to mechanical coupling with the wheels. Lin et al. present a power management strategy for a parallel hybrid vehicle.[8] In this strategy, the power split between the battery and the engine is obtained using an optimal control technique to maximize fuel economy and minimize emissions while maintaining the state of charge of the battery. The primary difference between the established work in the automotive industry and our problem is that our particular fuel cell cannot be throttled, requiring a more complex modeling mechanism than is used in the current system formulations.

More recently, Murphey et al. presented a power management scheme for a vehicle with multiple power sources.[9] Each individual source can be turned on or off, in addition to any throttling allowed by the device. Using a machine learning algorithm, the controller can decide at each time step which power sources are the best to use for a given state. While this algorithm has the same purpose as our algorithm, there are several key differences. First, the model assumes that the power sources can be turned on and off instantaneously, and, second, the optimization looks over a short time horizon and not over an entire mission profile.

2.2 Hybrid Control Systems

The field of hybrid control systems, consisting of both continuous and discrete dynamics, is well developed.[10,11] Using both types of dynamics, a much larger set of behaviors can be analyzed and modeled than using either type in isolation. In general, a hybrid system consists of a discrete state representing different modes of operation and continuous state representing physical parameters. The continuous dynamics depend on the current discrete state and the transition between discrete states can be constrained based on continuous state values.

In this paper, we use a hybrid automaton model.[12] This model encodes the discrete state of the system in a graph and the dynamics are defined for each node in the graph. Here, we present the discrete states graphically. The directed edges show possible state transitions, along with conditions that must be met for the transition to occur. In each discrete state, the evolution of the continuous state is written as $\dot{x} = f(x, t, u)$, where x is the continuous state, t is the current time and u is the model input. Additionally, we define the power output as a function of both the continuous and discrete states and the input.

3. EXAMPLE POWER COMPONENTS

In this section, we propose a power system model consisting of a 200 W fuel cell and a Li-ion battery. First we present the models of these system components using the framework of hybrid systems. These models are joined to form a model of the integrated power system. We look in particular at two types of models: full models used for simulation and simplified models that can be used for optimization.

3.1 Fuel Cell

The 200 W fuel cell power source was designed and manufactured by Ultra Electronics, Adaptive Materials, Inc (AMI). It is fueled by commercial propane canisters and consists of a 200 W solid oxide fuel cell, a fuel reformer, and a DC/DC converter. The propane gas is first desulfurized and then reformed via partial oxidation into a hydrogen-rich fuel stream to feed the fuel cell. The fuel cell was designed to be integrated with existing batteries on small unmanned ground vehicles, such as the TALON robot. This combined power system significantly increases the possible mission duration, especially under low power loads such as persistent stare missions.

Figure 1: TALON with Integrated Fuel Cell (Source: Ultra Electronics, AMI)

One of the challenges of integrating this power source is to develop an optimal duty cycle for using the fuel cell to recharge the batteries. Solid oxide fuel cells have significant warm-up and cool-down periods during which they consume power to run blowers or heating elements. The power consumption of the fuel cell during these periods becomes a crucial factor for optimization, since there is an energy cost associated with each on/off cycle of the fuel cell. To support this study, we conducted a preliminary assessment of the startup and shutdown power usage of the AMI 200-watt UGV fuel cell.

The fuel cell was connected to a TALON battery pack with a moderate state-of-charge (SOC) and issued a startup command. The current draw from the batteries was logged every 10 seconds until the fuel cell completed the startup procedure and began charging the batteries. Likewise, the fuel cell was then issued a shutdown command and the current draw was logged every 10 seconds until the fuel cell shut down. Power and energy values were calculated using the average voltage of the battery back (35 volts) throughout the tests. The power draw over time is shown in Figure 2 The fuel cell consumed approximately 6.5 Watt-hours over 16 minutes to start up, and approximately 5.3 Watt-hours over 18 minutes to shut down.

To model the operation of the fuel cell, we propose the hybrid model shown in Figure 3. The model consists of five discrete states, representing on, off and transitions. We divide the startup phase into two different discrete states q_1 and q_2 based on the power draw required and when fuel consumption begins. As seen in Figure 2, the input power decreases at about 300 seconds. We model two continuous states, time t and fuel level F. The time state is used to record how long the fuel cell has been in the shutdown or startup states and the transitions between the startup and shutdown states occur when the timer reaches an empirically determined value. The
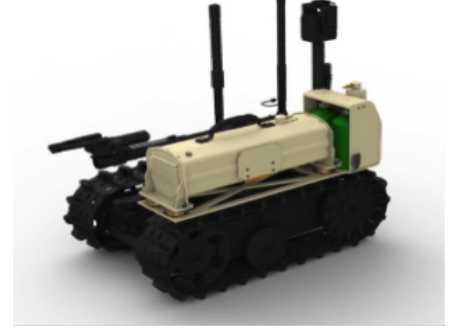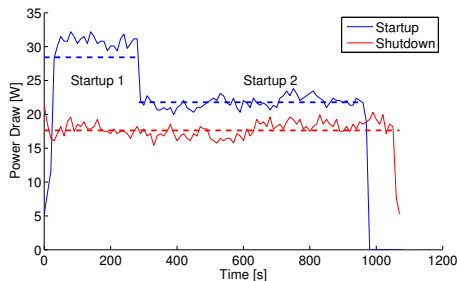

Figure 2: Power draws during startup and shutdown (dashed line- average value)
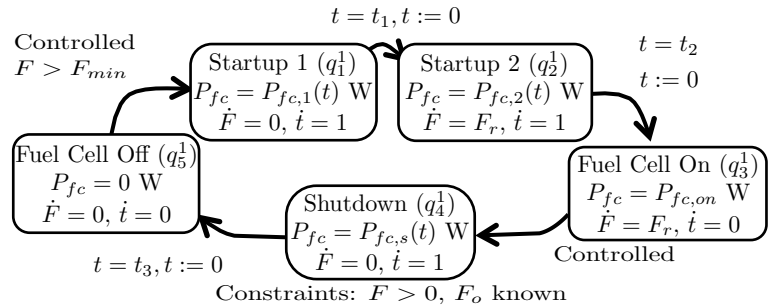
Figure 3: Hybrid model of fuel cell with discrete states
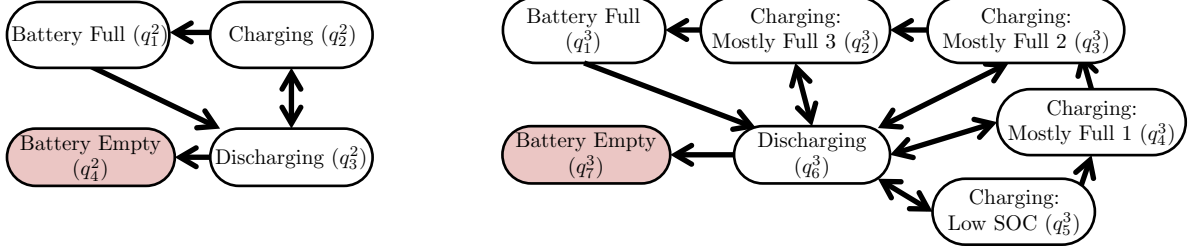
(a) Battery model showing the four basic states requiring nonlinear dynamics

(b) Battery model with discrete states representing charging levels, useful for averaged dynamics with constant power draw

Figure 4: Battery models

power draw also depends on the timer during startup and shutdown. For this fuel cell, the difference between an averaged model and the full empirical model is negligible.

3.2 Battery

The BB2590 battery pack is commonly used in military applications. For this research, we use the thermal-electric battery model presented by Kim et al.[13] The model has two continuous states, battery state of charge (SOC) and temperature T, and one input, battery current i. This model has been parameterized and validated against the BB2590 battery pack. The model is encoded in a SIMULINK module.

To enforce constraints on operation, we formulate a discrete state structure for the battery model shown in Figure 4a. The battery switches to the full state q_1^2 when $soc = 100\%$ and switches to the empty state q_4^2 when $soc = 0\%$. When the battery is full, the input current must be zero and if the current becomes negative (power drawn from the battery), the state switches to discharging. The transitions between charging and discharging are based on the battery current. In each discrete state, the dynamic functions for SOC and temperature are written $\dot{soc} = f_1(soc, T, i)$ and $\dot{T} = f_2(soc, T, i)$ respectively.

For our simplified model, we need dynamics to be of the form $\dot{soc} = k$, where k is a constant that is known for each discrete state. To make this simplification, the power draw must be constant since $\dot{soc}$ depends on the power output. At a constant power draw, the discharge rate $\dot{soc}$ varies little and can be approximated by the average discharge rate.

However, due to the required charging curve for the battery, the rate of charging decreases dramatically when the SOC gets close to 100%. As shown in Figure 5, the charge rate $\dot{soc}$ varies over the charging cycle. Averaging the dynamics over the entire charge cycle would result in significant model errors, especially if the battery started from a higher state of charge. To account for this change in our simplified model, we divide the charging state into a sequence of charging states, as shown in Figure 4b, with each state having dynamics of the form $\dot{soc} = k$. For this particular power charging level, we determined that three *Charging: Mostly Full* states was sufficient to model the SOC dynamics.

Most of the charging is done in the *Charging: Low SOC* state. However, once the SOC is sufficiently high, the charging constraints reduce the rate of charging (and the power used to charge). In this example, transition between *Low SOC* to *Mostly Full 1* was set at the point where the charging rate starts to decrease significantly. The rest of the transitions are chosen so that the variation in the charging rate is the same (i.e. in Figure 5, the difference between $\dot{soc}$ at the beginning and end of the *Mostly Full* segments is the same).

The number of *Mostly Full* states is based on desired fidelity of the model. As shown in Figure 5, the only significant deviation in SOC between the averaged and actual values occurs at very high state of charge. This linear model is sufficient for planning and optimization, which we will address in future work. Temperature dynamics can also be averaged, but would require many more states to sufficiently capture.

In addition to modeling battery operation, the full battery model can be used to estimate electrical efficiency. Using this model, we parameterized the efficiency of the battery based on SOC and the input current, as shown in Figure 6. These values were obtained by simulating the system with alternating charging and discharging current
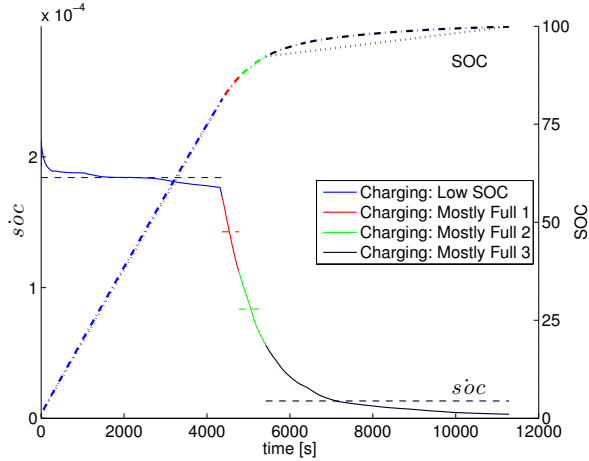
Figure 5: Comparing $\dot{soc}$ actual (solid) and averaged (dash) values for charging (150 W maximum). The battery SOC using the actual (dash-dot) and averaged (dot) values illustrates the four charging states.
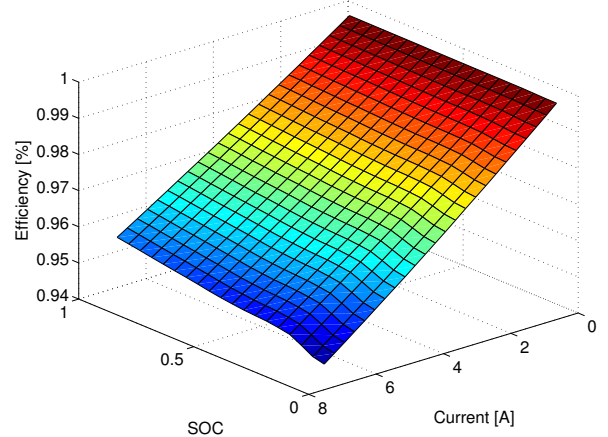

Figure 6: Battery efficiency as a function of SOC and current

of the same magnitude. The efficiency is calculated by comparing the power input to the power output. The upper current limit was chosen based on the maximum allowable charging current; efficiency values for higher discharge currents are obtained by extrapolation. Since the efficiency is roughly constant for a given current draw at different SOCs, we can average the efficiency in each discrete state for the simplified model as well.

3.3 Integrated Power System Model

Having defined the individual power models, we now present our integrated power system model. Figure 7 shows the basic interconnection of power sources. Each component produces a certain power P^i based on the input u^i. Some components might also consume power in certain circumstances. The sum of the individual outputs must produce sufficient power to meet UGV demand P_d. In a physical system, there are additional components that are required for the interconnection. These components can consume power. For simplicity, we assume that these are either negligible or modeled in conjunction with one of the individual components.
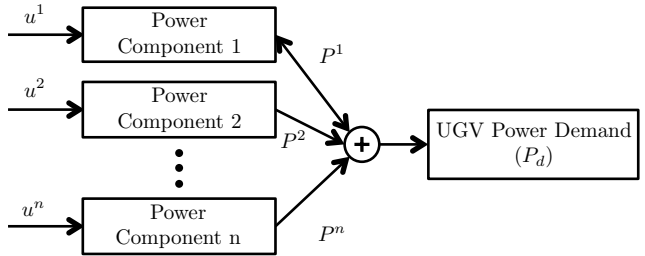

Figure 7: Interconnection of the power components

3.3.1 Power Demand

To determine the power requirements for the mission, we use a simulation model for the UGV operating in a known environment. This model includes motor models and track-terrain interaction models. From this model, we can simulate the desired mission and obtain the power demand over time P_d for a given mission. To allow for continuous operation, we assume that the averaged power demand $P_{d,avg} < P_{fc,on}$. Otherwise, the battery would eventually deplete, even with the fuel cell on, and leave the UGV incapacitated.

The driving loads can be decomposed into resistance due to terrain and changes in kinetic energy. We use the terrain model developed in by Guo and Peng[14] to model energy loss due to the terrain. Based on the current vehicle speed and turn rate, for a given terrain, the resulting resistance torques can be calculated. The model must be tuned for every different terrain of interest and is currently calculated for clay, sand, and sandy loam soils.
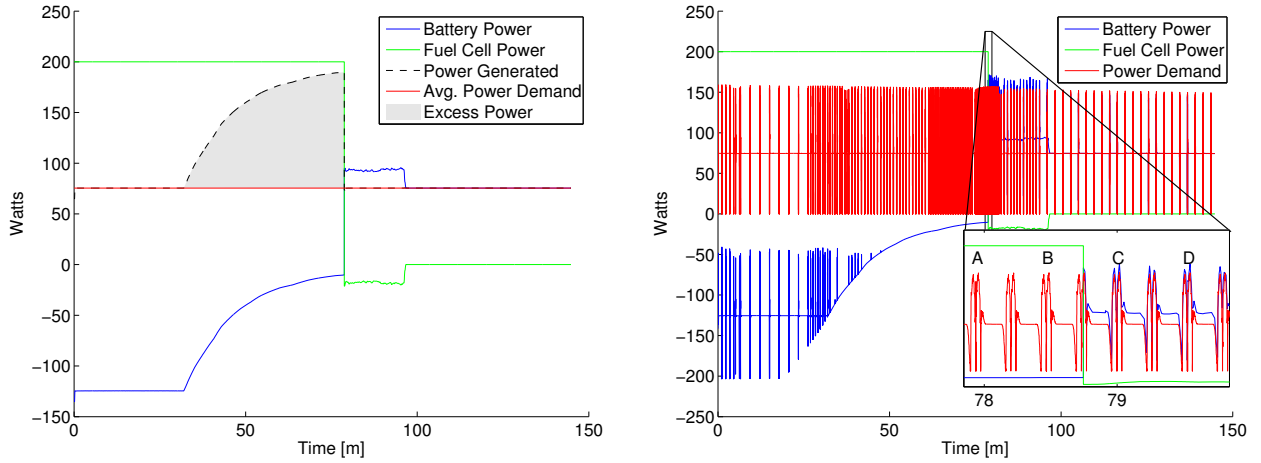
(a) Constant power demand, $P_d = 75.5$ W (b) Variable power demand

Figure 8: Simulating the power components for a variable-power and a constant-power mission

To provide appropriate torque inputs to the terrain model, we introduce a motor model. This model was obtained experimentally by testing iRobot Packbot motors. The model takes in the current shaft speed and the power being delivered to the motors and calculated the torque output. Together with a simple rigid body model of the UGV, we can simulate the UGV completing a mission and record the power used. In addition to variable power demands due to locomotion, electronic components on board require power for operation. We assume that these loads are known and constant over the entire mission.

While the full power demand can be used with nonlinear models, we are also interested in averaging the power demand to fit the constant power demand described in Section 3.2. This simplification assumes that the operating conditions, such as terrain and slope, are constant throughout the mission and that mission maneuvers are reasonably constant.

3.3.2 Power System Simulation

The nonlinear power system models described previously have been integrated in SIMULINK. Figure 8 shows the example power demand (P_d) trends for constant and variable power profiles. The first case, shown in Figure 8a, is based on a constant power mission, such as a persistent stare, where the power demand is constant. In general, persistent stare missions would have low power requirements, needing to only operate minimal electronic and communication loads. Previous experiments showed a 30 W power load while remaining stationary.[15] Additionally, we can approximate some variable power missions with an average power draw. For ease of comparison between the constant and variable power demands, the constant power demand P_d is set at the average power demand from the variable-power mission.

Figure 9: Portion of coverage path, letters correspond to Figure 8b

The variable power profile, shown in Figure 8b, is based on an area coverage mission. Using the method described by Broderick et al.,[16] we planned a reference path and trajectory for the coverage mission. Figure 9 shows a portion of the coverage path, with the robot moving from right to left. The marked locations correspond to Figure 8b, showing how the variation in power demand correspond to turning sections of the UGV's path, with the flat power demand sections corresponding to the straight travel sections.
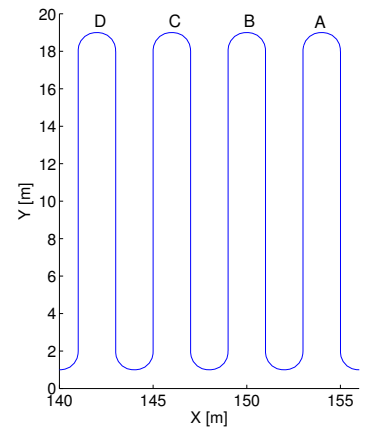
In both cases, the battery starts at 25% SOC. As the battery charges, it uses all the available power from the fuel cell until about 60 minutes into the mission. At this point, the SOC is sufficiently high that the battery must be charged at a lower rate, based on the known charging curve for
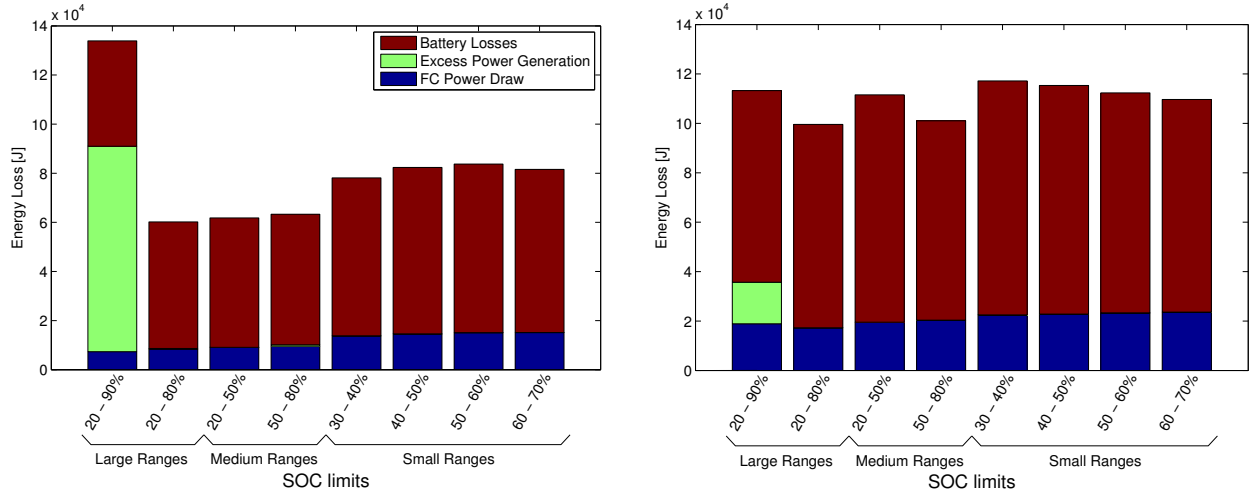
(a) $P = 40$ W, total energy usage: $1.25 \cdot 10^6$ J

(b) $P = 100$ W, total energy usage: $3.12 \cdot 10^6$ J

Figure 10: Energy losses for different SOC-based limits

the battery. In both missions, the maximum charging rate follows a similar curve, with some deviation in the variable power demand case. In the constant power mission, the total power demand is plotted, showing that the power generated (fuel cell power plus battery power) is greater than the power demand. This excess power generation represents a loss for the system and should be avoided. When the fuel cell switches off, at about 79 minutes, the fuel cell power becomes negative and the battery power exceeds the power demand. Once the shutdown period ends, the battery power output matches the power demand.

Both simulations use the full models of the battery and fuel cell. The simplified models can also be used to simulate the constant power mission. This simulation can be done faster to obtain estimates of power use.

4. COMPARISON OF CONTROL STRATEGIES

One use of the combined model presented in this paper is the comparison of system performance over a simulated mission. In this section, we consider two different system performance characteristics: energy loss and thermal behavior. Both can have a large impact on the operation of a UGV in a mission. If energy losses are significant, the range of the UGV is limited. If thermal constraints are not met, the UGV can be incapacitated in the middle of a mission, resulting in a potentially dangerous recovery or loss of vehicle. The results from this section can be used as a basis for mission planning or optimization.

We consider the previously described battery/fuel cell hybrid power system. The control of the fuel cell is based on the current battery SOC: when the battery reaches a low SOC threshold, the fuel cell is turned on and when the SOC reaches the higher threshold, the fuel cell is turned off. Mission time or power demand does not influence the control decision. For these simulations, we use nonlinear models.

4.1 Energy Efficiency

As discussed in the previous sections, we consider three sources of energy loss: battery losses, fuel cell power draws (during startup and shutdown) and excess power generated by the fuel cell (see shaded area in Figure 8a, for example). Here we consider the two power demand levels shown in Figure 10. This figure shows the total energy lost over a 8.6 hr mission. In all of these tests, the battery begins at 50% SOC and the fuel cell is initially on.

Figure 10 shows the energy lost for several different control law SOC thresholds. The first two represent large SOC ranges for battery operation (20-90% and 20-80% respectively). These cases have the smallest losses due to the battery and the fuel cell power draw, but in the cases with the high threshold at 90% SOC, there is a region where excess power is generated by the fuel cell that is not needed for charging or for the mission. The different

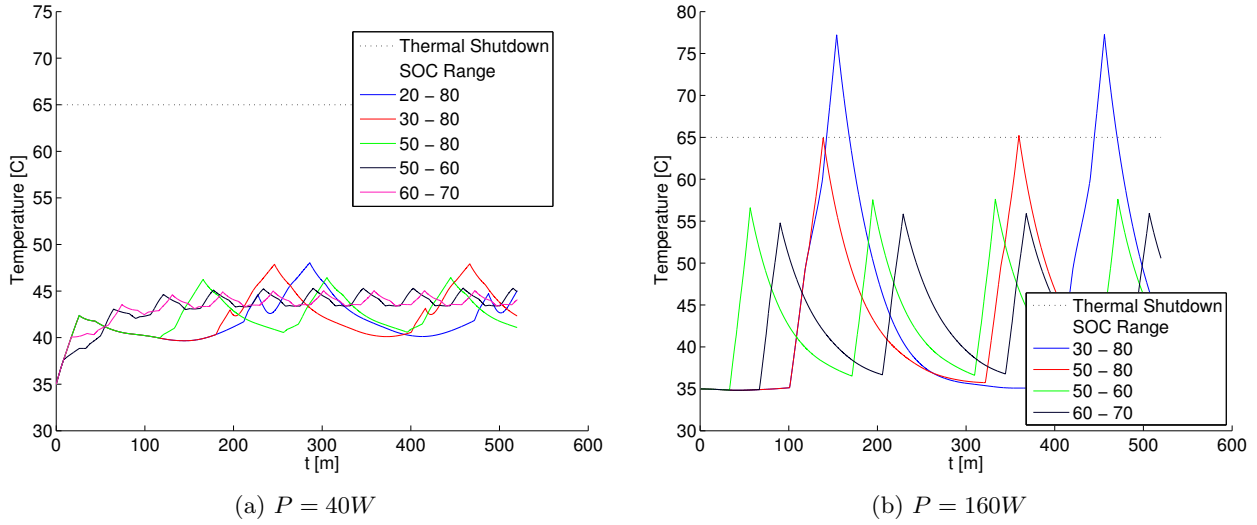(a) $P = 40W$ (b) $P = 160W$

Figure 11: Comparing thermal response under different power conditions using a SOC-based control strategy

power demand levels are identical in this regard, though the excess energy generated is significantly smaller at the higher power demand.

The other tests show medium sized SOC ranges (20-50% and 50-80%) and small ranges (30-40%, 40-50%, 50-60%, and 60-70%). These cases shows higher losses due to the fuel cell power draw, but the overall losses depend on the mission power demand. For the lower power demand, the larger ranges have less overall energy loss and there is minimal difference between energy lost within each group of ranges. At the higher power demand, there are visible trends within the medium- and small-range groups. In each of these cases, the range with the higher limits has lower energy usage, due to the higher efficiency of the battery at higher SOC. In fact, when using the 50-80% SOC range, the higher efficiency almost balances the additional fuel cell power draw compared to the 20-80% SOC range.

These observations suggest that operating the fuel cell for as long as possible in each cycle yields the most efficient operation from an energy perspective. However, if the SOC becomes too high, significant amounts of energy is lost due to the inability of the battery to accept power rapidly. Also, the fuel cell must be restarted in time for the startup phase to be completed before the battery is fully depleted. Increasing power demand requires a higher activation threshold for turning on the fuel cell. For the 40 W and 100 W cases, the minimum lower SOC thresholds are about 9% and 17% respectively.

4.2 Thermal Behavior

Battery thermal behavior is also an important consideration for UGVs.[13] When operating in environments with high ambient temperatures for extended periods of time, battery overheating is a possibility. For some batteries, including the BB2590 studied in this system, the batteries are designed to shutdown before critical temperatures are reached. The sources of heat generation include battery resistance and entropic heating (during discharge). Heat is dissipated to the ambient air and the battery exhibits entropic cooling during charging. While the fuel cell could be used while the battery is inoperable, this must be considered in the control strategy so that the fuel cell completes its startup sequence before the battery overheats.

To simulate the thermal response of the system, we used a constant power demand, as described in the Section 4.1, as well as the same SOC-based control for the fuel cell. The mission duration is also about 8.6 hrs. At the beginning of the mission, the battery temperature is 35° C, which is also the ambient temperature for the mission. We assume that the ambient temperature remains at 35° C over the entire mission. Figure 11 shows the temperature over time for two different power levels: 40 W and 160 W. In the case of low power demand, there is little difference in maximum temperature at the different control strategies. None of the runs exceed the temperature threshold for thermal shutdown.

In the case of higher power demand, the thermal threshold is exceeded when the more energy efficient (larger SOC range) is followed. While there are still large temperature spikes while operating at smaller ranges, the spikes are much smaller, though more frequent. It is important to note that the rapid decreases in battery temperature are mostly heat loss to the ambient environment. While the battery is charging, the rate of charging is very low and little heat is being generated due to battery resistance.

Comparing thermal behavior under the 50-60% range with the 60-70% range shows some correlation between energy efficiency and thermal behavior; the 60-70 % range has smaller temperature spikes and higher energy efficiency. This suggests that for similar SOC ranges, the energy efficiency does correlate to lower temperature, but that in different SOC ranges, the effects are not so obvious.

5. CONCLUSIONS

In this paper, we have presented a modeling framework for UGVs with multiple power systems. The hybrid modeling strategy allows individual components to be modeled and integrated to simulate a UGV mission. Studying a simple fuel cell/battery hybrid, we have shown how this framework can be used to evaluate the performance of different control laws for desired criteria. In particular, we investigated energy losses of the entire power system and thermal response of the battery for an extended UGV mission.

Future work includes using this combined model to plan and optimize energy efficiency for a mission. We also plan to validate these models by running physical experiments with a UGV carrying a fuel cell and batteries running the controllers described in this paper.

ACKNOWLEDGMENTS

REFERENCES

[1] Wilhelm, A. N., Surgenor, B. W., and Pharoah, J. G., "Design and evaluation of a micro-fuel-cell-based power system for a mobile robot," *Mechatronics, IEEE/ASME Transactions on* **11**(4), 471–476 (2006).

[2] Joh, H.-I., Ha, T. J., Hwang, S. Y., Kim, J.-H., Chae, S.-H., Cho, J. H., Prabhuram, J., Kim, S.-K., Lim, T.-H., Cho, B.-K., Oh, J.-H., Moon, S. H., and Ha, H. Y., "A direct methanol fuel cell system to power a humanoid robot," *Journal of Power Sources* **195**(1), 293 – 298 (2010).

[3] Chan, C., "The state of the art of electric, hybrid, and fuel cell vehicles," *Proceedings of the IEEE* **95**(4), 704–718 (2007).

[4] Khaligh, A. and Li, Z., "Battery, ultracapacitor, fuel cell, and hybrid energy storage systems for electric, hybrid electric, fuel cell, and plug-in hybrid electric vehicles: State of the art," *Vehicular Technology, IEEE Transactions on* **59**(6), 2806–2814 (2010).

[5] Rodatz, P., Paganelli, G., Sciarretta, A., and Guzzella, L., "Optimal power management of an experimental fuel cell/supercapacitor-powered hybrid vehicle," *Control Engineering Practice* **13**(1), 41–53 (2005).

[6] Ceraolo, M., Di Donato, A., and Franceschi, G., "A general approach to energy optimization of hybrid electric vehicles," *Vehicular Technology, IEEE Transactions on* **57**(3), 1433–1441 (2008).

[7] Barsali, S., Miulli, C., and Possenti, A., "A control strategy to minimize fuel consumption of series hybrid electric vehicles," *Energy Conversion, IEEE Transactions on* **19**(1), 187–195 (2004).

[8] Lin, C.-C., Peng, H., Grizzle, J., and Kang, J.-M., "Power management strategy for a parallel hybrid electric truck," *Control Systems Technology, IEEE Transactions on* **11**(6), 839–849 (2003).

[9] Murphey, Y. L., Chen, Z., Kiliaris, L., and Masrur, M. A., "Intelligent power management in a vehicular system with multiple power sources," *Journal of Power Sources* **196**(2), 835 – 846 (2011).

[10] Goebel, R., Sanfelice, R. G., and Teel, A. R., "Hybrid dynamical systems," *Control Systems* **29**(2), 28–93 (2009).

[11] Branicky, M. S., "Introduction to hybrid systems," in [*Handbook of Networked and Embedded Control Systems*], *Control Engineering*, 91–116, Birkhuser Boston (2005).

[12] Alur, R., Courcoubetis, C., Halbwachs, N., Henzinger, T., Ho, P.-H., Nicollin, X., Olivero, A., Sifakis, J., and Yovine, S., "The algorithmic analysis of hybrid systems," *Theoretical Computer Science* **138**(1), 3 – 34 (1995).

[13] Kim, Y., Siegel, J., and Stefanopoulou, A., "A computationally efficient thermal model of cylindrical battery cells for the estimation of radially distributed temperatures," in [*American Control Conference (ACC), 2013*], 698–703 (2013).

[14] Guo, T. and Peng, H., "A simplified skid-steering model for torque and power analysis of tracked small unmanned ground vehicles," in [*American Control Conference (ACC)*], 1106–1111 (2013).

[15] Broderick, J., Tilbury, D., and Atkins, E., "Energy usage for UGVs executing coverage tasks," in [*Proc. SPIE 8387*], (2012).

[16] Broderick, J. A., Tilbury, D. M., and Atkins, E. M., "Optimal coverage trajectories for a UGV with tradeoffs for energy and time," *Autonomous Robots* **36**(3) (2014).